JANUSZ SZMYD**[1], MARIAN BRANNY*, MICHAL KARCH*, WALDEMAR WODZIAK*,
MAREK JASZCZUR**, REMIGIUSZ NOWAK**

EXPERIMENTAL AND NUMERICAL ANALYSIS OF THE AIR FLOW IN T-SHAPE CHANNEL FLOW

EKSPERYMENTALNA I NUMERYCZNA ANALIZA PRZEPŁYWU POWIETRZA PRZEZ SKRZYŻOWANIE KANAŁÓW W KSZTAŁCIE LITERY T

This paper presents the results of experimental and numerical investigations of air flow through the crossing of a mining longwall and ventilation gallery. The object investigated consists of airways (headings) arranged in a T-shape. Maintained for technological purposes, the cave is exposed particularly to dangerous accumulations of methane.

The laboratory model is a certain simplification of a real longwall and ventilation gallery crossing. Simplifications refer to both the object's geometry and the air flow conditions. The aim of the research is to evaluate the accuracy with which numerical simulations model the real flow. Stereo Particle Image Velocimetry (SPIV) was used to measure all velocity vector components. Three turbulence models were tested: standard k-ε, k-ε realizable and the Reynolds Stress Model (RSM). The experimental results have been compared against the results of numerical simulations. Good agreement is achieved between all three turbulence model predictions and measurements in the inflow and outflow of the channel. Large differences between the measured and calculated velocity field occur in the cavity zone. Two models, the standard k-ε and k-ε realizable over-predict the measure value of the streamwise components of velocity. This causes the ventilation intensity to be overestimated in this domain. The RSM model underestimates the measure value of streamwise components of velocity and therefore artificially decreases the intensity of ventilation in this zone. The RSM model provides better predictions than the standard k-ε and k-ε realizable in the cavity zone.

Keywords: T-shape channel flow, PIV, validation of CFD codes, mining ventilation

Przedmiotem badań jest walidacja wybranych modeli CFD (Computational Fluid Dynamics) przy przepływie powietrza przez laboratoryjny model skrzyżowania kanałów w kształcie litery T. Stanowisko laboratoryjne przedstawia uproszczony model skrzyżowania ściany z chodnikiem wentylacyjnym. Przy-

* AGH UNIVERSITY OF SCIENCE AND TECHNOLOGY, FACULTY OF MINING AND GEOENGINEERING, AL. A. MICKIEWICZA 30, 30-059 KRAKOW, POLAND
** AGH UNIVERSITY OF SCIENCE AND TECHNOLOGY, DEPARTMENT OF FUNDAMENTAL RESEARCH IN ENERGY ENGINEERING, FACULTY OF ENERGY AND FUELS, AL. A. MICKIEWICZA 30, 30-059 KRAKOW, POLAND
[1] CORRESPONDING AUTHOR: AGH UNIVERSITY OF SCIENCE AND TECHNOLOGY, DEPARTMENT OF FUNDAMENTAL RESEARCH IN ENERGY ENGINEERING, FACULTY OF ENERGY AND FUELS, AL. A. MICKIEWICZA 30, 30-059 KRAKOW, POLAND; E-mail address: janusz.szmyd@agh.edu.pl

jęto, że przepływ powietrza jest ustalony i izotermiczny. Dla tych warunków z równości liczb Reynoldsa w modelu i obiekcie rzeczywistym wynika warunek podobieństwa uśrednionych pól prędkości (przy założeniu nieściśliwości powietrza).

Pomiar składowych wektora prędkości wykonano metodą SPIV (Stereo Particle Image Velocimetry). W pracy testowano trzy modele turbulencji: standardowy model *k-ε*, jego modyfikację *k-ε „realizable"* oraz model naprężeń Reynoldsa (Reynolds Stress Model). Obliczenia numeryczne dla warunków identycznych jak w eksperymencie wykonano przy zastosowaniu programu FLUENT. Zadawalającą zgodność pomiędzy pomiarami i obliczeniami wszystkimi trzema modelami turbulencji uzyskano w kanałach zarówno po stronie dopływu jak i wypływu strumieniem powietrza ze skrzyżowania. Natomiast w strefie wnęki żaden z testowanych modeli nie wykazał pełnej zgodności z wynikami eksperymentalnymi.

Do oszacowania dokładności z jaką symulacje numeryczne odwzorowują przepływ rzeczywisty w strefie wnęki wykorzystano wskaźnik charakteryzujący czas zaniku cząstek znacznikowych wprowadzonych do przepływu. Obliczenia wykonano dla dwóch modeli turbulencji: standardowego *k-ε* oraz modelu RSM. Czas potrzebny do rozrzedzenia początkowej koncentracji gazu znacznikowego do określonego poziomu – w przedziale koncentracji względnej od 0,3 do 0,1 – uzyskany z obliczeń standardowym modelem *k-ε* jest krótszy o 32%-27% od czasu wynikającego z pomiarów podczas gdy model RSM przeszacowuje wartości mierzone wartości koncentracji gazu o 18%-27%. Dwa z testowanych modeli, mianowicie standardowy *k-ε* i *k-ε „realizable"* przeszacowują mierzone wartości składowych wzdłużnych wektora prędkości. Konsekwencją tego jest sztuczne zawyżenie intensywności wentylacji we wnęce. Z kolei model RSM niedoszacowuje mierzone wartości składowych wzdłużnych wektora prędkości co powoduje zaniżenie rzeczywistej intensywności wentylacji tej strefy. Z przeprowadzonych badań wynika, że w obszarze wnęki rezultaty uzyskane modelem RSM są bliższe do wartości mierzonych niż prognozowane standardowym modelem *k-ε* i modelem *k-ε „realizable"*.

Słowa kluczowe: przepływ przez skrzyżowanie kanałów o kształcie T, PIV, walidacja kodów CFD, wentylacja kopalń

1. **Introduction**

Flow and mixing at a T-shape channel is encountered in many industrial applications such as mining ventilation systems, chemical reaction processes, combustion processes, and plant piping systems (Haven & Kurosaka, 1977; Kelso et al., 1996; Nakayama et al., 2005). Adopting several simplification assumptions, the crossing of the longwall with the ventilation gallery can also be treated as a system of T-shape ventilation channel flow. The geometry of the intersection of the mining face and ventilation gallery is shown in figure 1. While this geometry is apparently simple, the flows generated in T-shape channels are often complex. Depending on the Reynolds number, a large separation zone can be formed, behind the right corner of the T-junction (see Fig. 1). On the other hand, on the left side of the T-junction (which actually has the form of a cavity, see Fig. 1) another recirculation zone of totally different behavior can be formed. The complexity of these recalculation zones makes the numerical prediction of the flow very difficult. The flow structure behind the right corner of the T-junction (see Fig. 1) itself is very complex from an experimental point of view. Across the channel, very large velocity near the outer walls of the channel and very low or negative velocity near the inner walls can be found. This is no trivial obstacle to achieving good accuracy using PIV (Particle Image Velocimetry) (Jaszczur et al., 2011).

The thermo-fluid behaviors of cross-flow type T-junctions have been experimentally/numerically investigated elsewhere (Nakayama et al., 2007; Jaszczur et al., 2012a, 2012b). Numerous papers have been published on periodic, straight or L-shaped turbulent channels using a wide variety of modeling techniques: RANS, URANS, LES, DLES and DNS (Jaszczur & Portela, 2008; Kuan et al., 2007; Mossad et al., 2009). However, there are small number of detailed ex-

perimental studies related to the single phase air flow and gas-particulate two-phase turbulent flow L-shaped channels (Humphery et al., 1981; Taylor et al., 1982).

This paper investigates the air flow through the crossing of the T-shaped duct. The laboratory model is a certain simplification of the crossing of the mining longwall and ventilation gallery. Simplifications refer both to the object's geometry (the rectangular shape of the cross-sections of workings, the smooth walls of the channel and without mining face equipment) and to the flow conditions (without the inflow of air from the goaf area).

The model consists of airways (headings) arranged in a T-shape. Maintained for technological reasons, the cave is exposed particularly to dangerous accumulations of methane. A methane-air mixture flows into a cave of 3-5 m length from a goaf space. This flow is not limited, because it should push away the zone of high methane concentrations from the conveyor drive located at the terminal section of the wall. The existing system of duct connections causes this to be the least ventilated part of the longwall. Properly arranged ventilation should assure the maintenance of methane concentrations at a safe level.

For this type of flow, numerical investigations are typically performed based on viscosity turbulence models with the standard k-ε model (Aminossadati & Hooman, 2008; Krawczyk, 2007; Silvester et al., 2002; Branny & Filipek, 2008)

The validation test for CFD simulation for flow and methane concentration in the face area was done in the US (Wala et al., 2001, 2007). Depending on the excavation system, the authors suggested various models for the best way to simulate the real flow-namely, the RNG k-ε model, the k-ω model in the SST version and the Spalart-Allmaras model. The flow field investigated in this paper differs significantly from those analyzed in the above mentioned papers, where the connections between the ventilation ducts were arranged differently. This paper investigates the air flow through the crossing of the T-shaped duct.
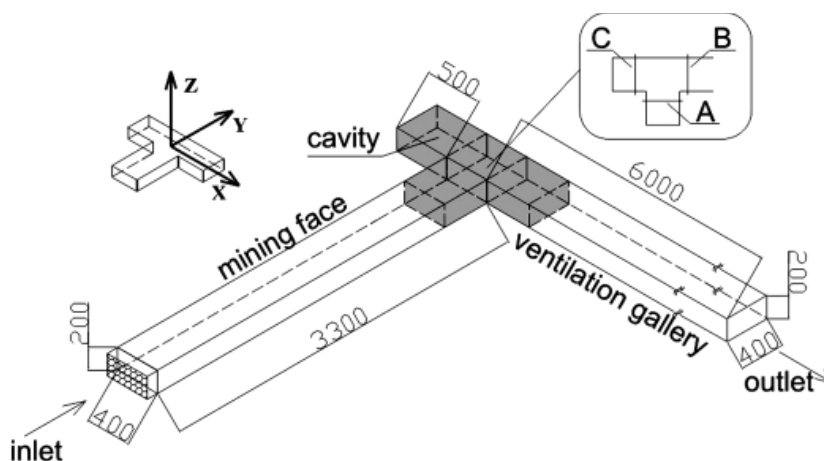

Fig. 1. Experimental set-up of T-shape channel flow

2. Experimental setup

The experimental set-up shown in figure 1 represents a model of the intersection of the mining face and ventilation gallery. The dimensions of the real object are assumed to be: the cross-section of the duct a 4 m × 2 m duct cross-section, the length of a 5-m-long cavity, the length of a 3.3-m inlet section (terminal segment of a mine face) and a 5.8-m outlet. The mean velocities are usually in the range of 1-2 m/s (Reynolds number from 150,000 to 300,000). The geometrical scale of the physical model was 1:10. It was assumed that the air flow is steady and isothermal. In this case, the equality of the Reynold's number in the model and the real object ensures that the flow criteria are similar.

Air was used as the experimental fluid in the channel, thus the equality of the Pr number was automatic. Having equal Re numbers ensures that the averaged velocity fields are similar. The inlet velocity was $U = 9.85$ m/s and the corresponding Reynolds number was equal to Re = 148,600. Stereo Particle Image Velocimetry (SPIV) was used to evaluate the velocity vector components and the particles were illuminated with a double-pulse Nd:YAG laser of energy of about 400 mJ per pulse. The digital images were acquired using a 4 Mpx monochromatic CCD camera. In each experiment, 1000 double frame images were recorded with a camera recording at a frequency of 3 Hz, which resulted in an overall time for one measure of around 5 minutes. Time Δt between two subsequent frames varied from about 100 μs to 500 μs. However, the measurements inside the cave were taken in the range of 3000-4000 μs, because the velocities there are lower than in the other sections. During the calculations, the size of the interrogation windows that exhibit satisfying results was set at 32 × 32 px.

3. Mathematical model

Classical modeling of turbulence is based on the Reynolds concept, which for incompressible and Newtonian fluids yields the following equations (Rodi, 1979)

$$\frac{\partial U_i}{\partial x_i} = 0 \tag{1}$$

$$\frac{\partial U_i}{\partial t} + U_j \frac{\partial U_i}{\partial x_j} = -\frac{1}{\rho}\frac{\partial P}{\partial x_i} + \frac{\partial}{\partial x_j}\left(v\frac{\partial U_i}{\partial x_j} - \overline{u_i u_j}\right) \tag{2}$$

$$-\overline{u_i u_j} = v_t\left(\frac{\partial U_i}{\partial x_j} + \frac{\partial U_j}{\partial x_i}\right) - \frac{2}{3}\rho k \delta_{ij}$$

where: $v_t = C_\mu \dfrac{k^2}{\varepsilon}$ is the turbulent viscosity, k is kinetic energy, ε is the dissipation rate of k, C_μ is the constant, δ_{ij} the Kronecker delta, U_i and u_i the mean and fluctuating components of velocity, ρ the density, P the pressure, and v *the* molecular viscosity.

In this study, three models of turbulence were tested: the standard k-ε model, a variation of that model, the k-ε realizable model and the Reynolds stress model. The standard k-ε model is

the most widely used turbulent model for solving industrial problems, particularly in mining for solving ventilation problems. This is a semi-empirical model based on the Bossinesq's conception of turbulent viscosity and on two transport equations for turbulent kinetic energy and its dissipation rate (equations (3) and (4)).

$$\frac{\partial k}{\partial t} + U_i \frac{\partial k}{\partial x_i} = \frac{\partial}{\partial x_i}\left(\left(\nu + \frac{\nu_t}{\sigma_k}\right)\frac{\partial k}{\partial x_i}\right) - \overline{u_i u_j}\,\frac{\partial U_i}{\partial x_j} - \varepsilon \tag{3}$$

$$\frac{\partial \varepsilon}{\partial t} + U_i \frac{\partial \varepsilon}{\partial x_i} = \frac{\partial}{\partial x_i}\left(\left(\nu + \frac{\nu_t}{\sigma_\varepsilon}\right)\frac{\partial \varepsilon}{\partial x_i}\right) - C_1 \frac{\varepsilon}{k}\overline{u_i u_j}\,\frac{\partial U_i}{\partial x_j} - C_2 \frac{\varepsilon^2}{k} \tag{4}$$

where C_1, C_2, σ_k, σ_ε are constants (Rodi, 1979).

The k-ε realizable model satisfies certain mathematical constrains on the Reynolds stresses, and is consistent with the physics of turbulent flow. This model is recommended for flows involving rotation, separation, re-circulation and for boundary layers with strong adverse pressure gradients. The Reynolds Stress Model (RSM) closes two systems of equations (1), (2) by solving transport equations for Reynolds stresses, together with an equation for the dissipation rate. The RSM is expected to give most accurate predictions for complex turbulent flows.

A two-layer-based, non-equilibrium wall function was used in the near-wall region. A two-layer approach is recommended for complex flows that involve flow separation, flow reattachment and flow impingement for its ability to account for the effects of pressure gradients in the wall-neighboring cells.

The air flow for conditions similar to experimental investigations was numerically simulated using FLUENT software.

4. Mesh size

A structured, non-uniform mesh was generated for the computational domain. Local refinement was used in the cross-road region, where large gradients exist in the flow field and in the vicinity of the walls. Three different size meshes of about 1,000,000, 2,800,000 and 4,000,000 cells were examined. Figure 2 and 3 present the streamwise velocities at four locations in the cavity zone (C) and in the downstream zone (B) obtained using the standard k-ε model with different mesh sizes. The most visible effects of mesh refinement may be observed in cross-sections further apart from the sharp corners of the crossing, especially in the cavity zone and the results for two finer meshes differ slightly in comparison with the coarse one. Thus, the mesh consisting of 4,000,000 cells was used in further calculations.
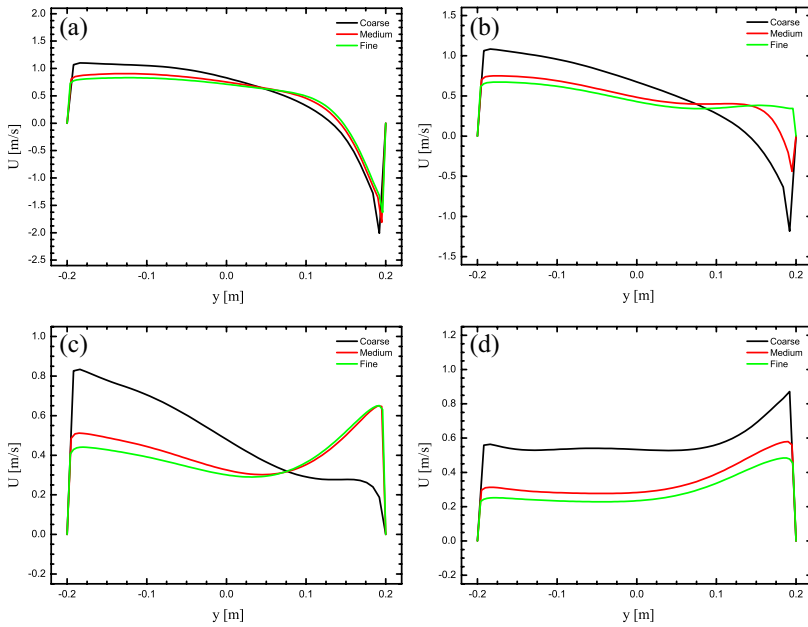
Fig. 2. The effect of mesh refinement on the numerical prediction of the streamwise velocity in cavity (zone C) at $z = 0.0$ and $x = -0.3$ (a), $z = 0.0$ and $x = -0.4$ (b), $z = 0.0$ and $x = -0.5$ (c), $z = 0.0$ and $x = -0.6$ (d)
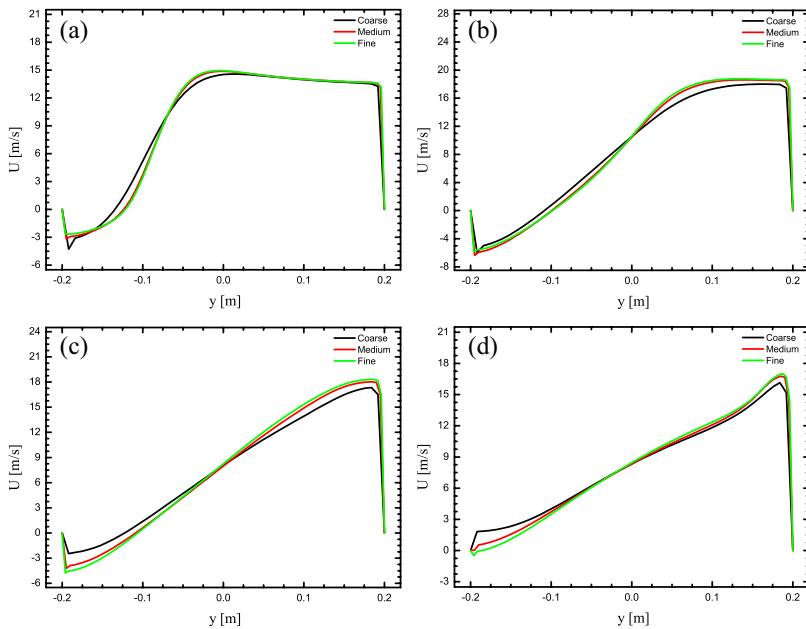
Fig. 3. The effect of mesh refinement on the numerical prediction of the streamwise velocity in outflow zone B at $z = 0.0$ and $x = 0.3$ (a), $z = 0.0$ and $x = 0.6$ (b), $z = 0.0$ and $x = 0.9$ (c), $z = 0.0$ and $x = 1.2$ (d)

5. Experimental and numerical results

The measurements and calculations were performed for the flow velocity 9.85 m/s (Reynolds number 148,600). We present here only the profiles of stream-wise and wall-normal components of velocity along the horizontal line at $z = 0.0$ and $z = 0.05$ located in zones A, B and C using the following labeling: SKE – standard k-ε model, RKE-k-ε realizable model, RSM – Reynolds Stress Model.

Inlet, (zone A)

Figure 4 shows the velocities for Zone A just before the channels intersection at a distance of 0.1 m ($x = -0.3$) from the corners. In this section, the calculations are in good agreement with experimental results.
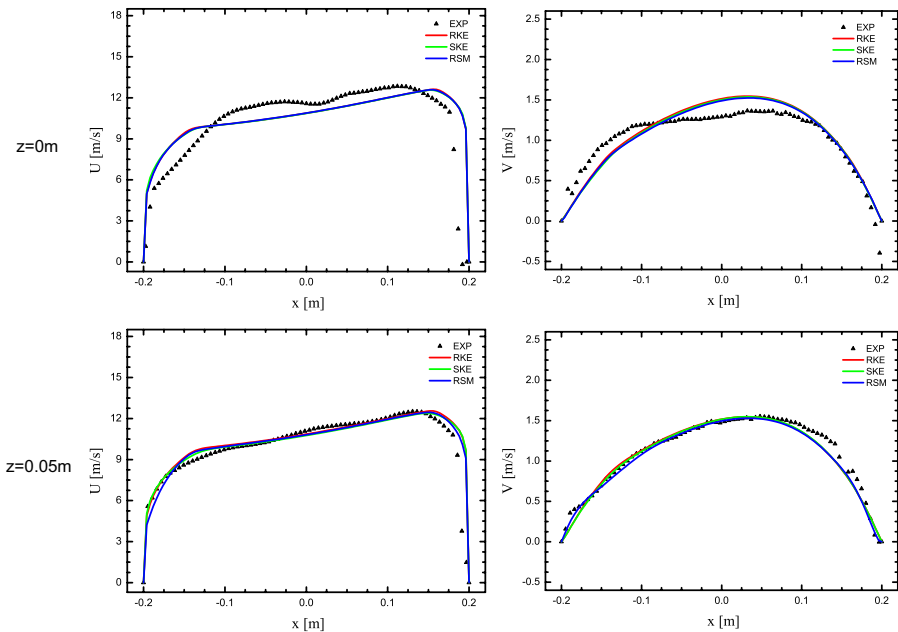
Fig. 4. Flow streamwise (left) and wall-normal (right) velocity components along
a horizontal line at $x = -0.3$ (for labeling see the text)

Outflow (zone B)

Figure 5, 6, 7 and 8 show the comparison of measured and calculated velocity along two horizontal lines and at four different locations behind the sharp elbow downstream. The cross-sections in zone B (Fig. 1) are located at a distance equal to 0.1 m, 0.4 m, 0.7 m and 1.0 m from the right corner of the intersection. None of the turbulent models matched the experimental data. For streamwise velocity components, the differences between measurements and calculations data increase with the increasing distance from the right corner of the intersection and the calculated
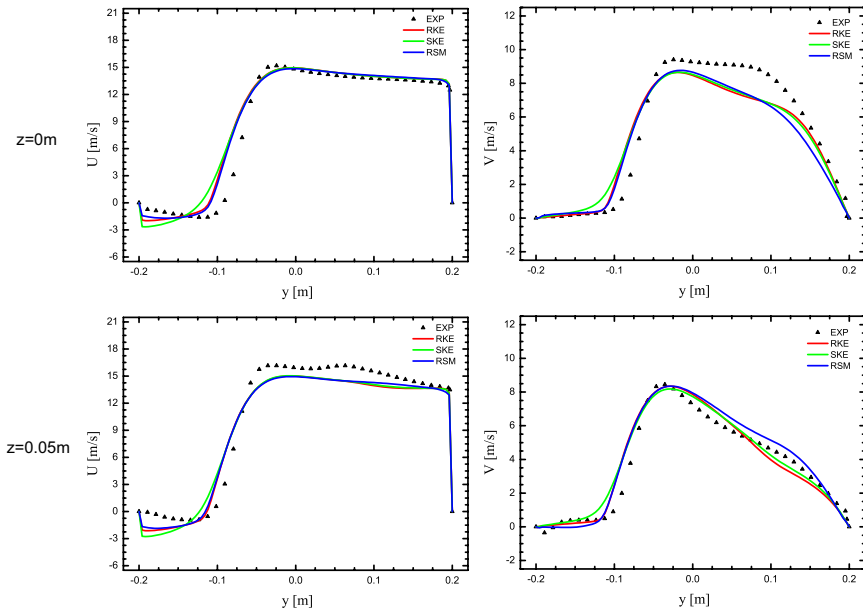
Fig. 5. Comparison for streamwise (left) and wall-normal (right) velocity components along a horizontal line at the middle ($z = 0.00$ m) and top ($z = 0.05$ m) of the duct heights and at the distance 0.1 m ($x = 0.3$) from the right corner of the crossing
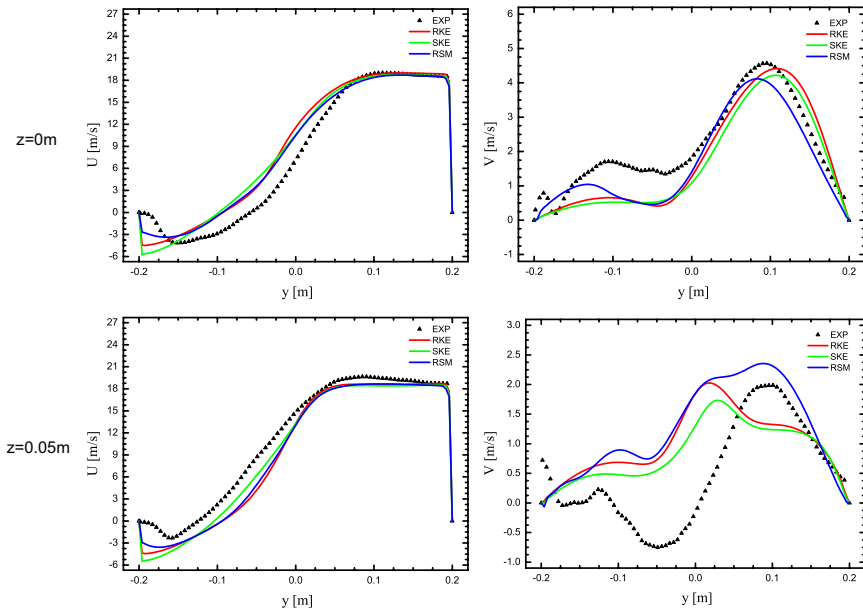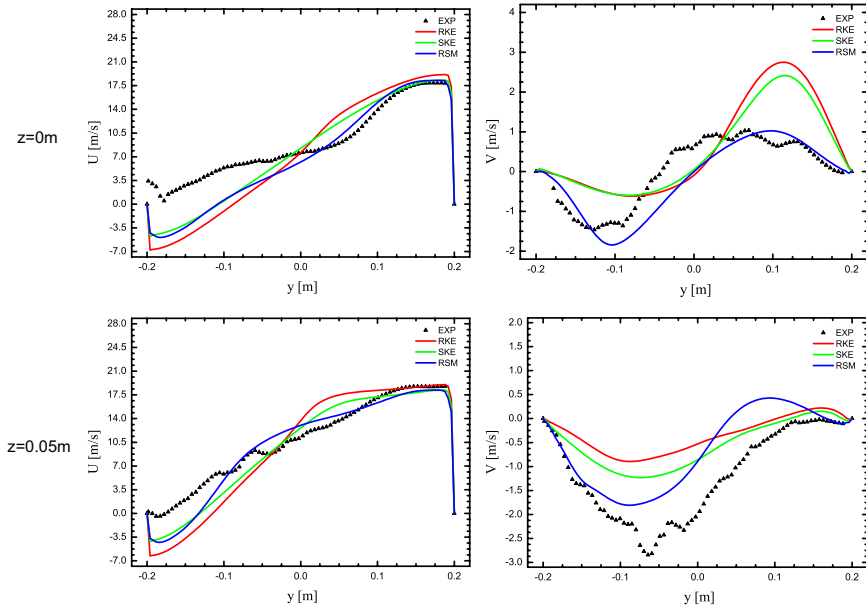

Fig. 6. Comparison for streamwise (left) and wall-normal (right) velocity components along a horizontal line at the middle ($z = 0.00$ m) and top ($z = 0.05$ m) of the duct heights and at the distance 0.4 m ($x = 0.7$) from the right corner of the crossing

Fig. 7. Comparison for streamwise (left) and wall-normal (right) velocity components along
a horizontal line at the middle ($z = 0.00$ m) and top ($z = 0.05$ m) of the duct heights
and at the distance 0.7 m ($x = 0.9$) from the right corner of the crossing
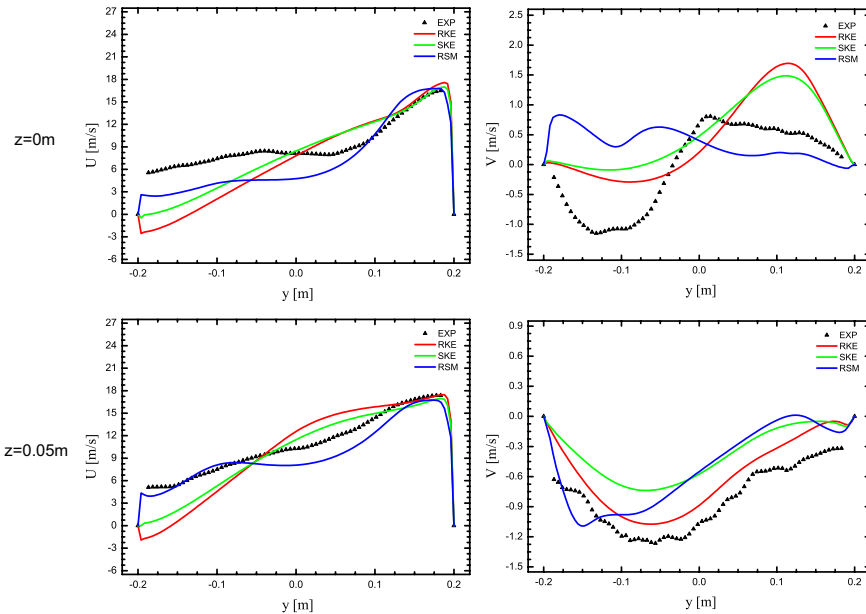

Fig. 8. Comparison for streamwise (left) and wall-normal (right) velocity components along
a horizontal line at the middle ($z = 0.00$ m) and top ($z = 0.05$ m) of the duct heights
and at the distance 1.0 m ($x = 1.2$) from the right corner of the crossing

values over-predict the negative streamwise components in the zone with recirculation. In turn, the normal components of velocity, the differences between calculation and measurements data change from cross-section to cross-section. Due to the accuracy required for ventilation problems, it can be concluded that the numerical predictions reflect the real flow with sufficient precision for practice in the outflow section and that all tested turbulent models behaved very similarly to each other in this zone.

Cavity (zone C)

The experimental and calculated values of the streamwise and normal components of velocity at four different locations in the cavity area are presented in Figures 9, 10, 11 and 12. The cross-sections in zone C (Fig. 1) are located at a distance of 0.1 m, 0.2 m, 0.3 and 0.4 m from the left corner of the intersection. In this domain, the difference between the measured results and the
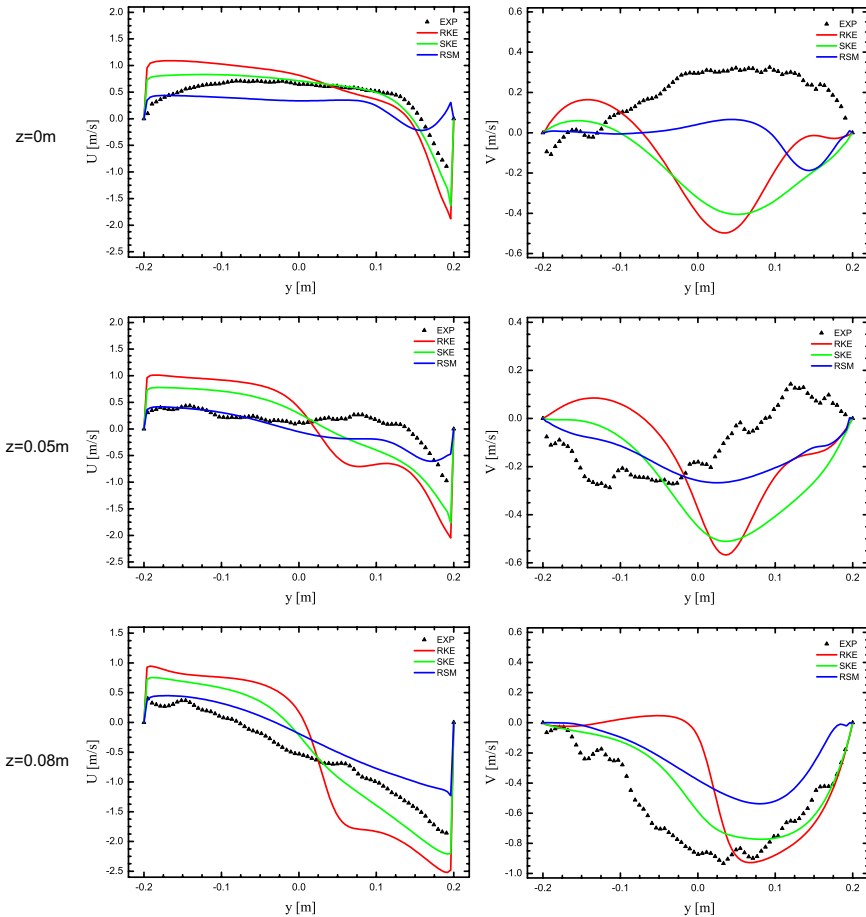

Fig. 9. Comparison for streamwise (left) and wall-normal (right) velocity components along a horizontal line at $z = 0.00$, $z = 0.05$, $z = 0.02$ and the distance 0.1 m ($x = -0.3$) from the left corner of the crossing
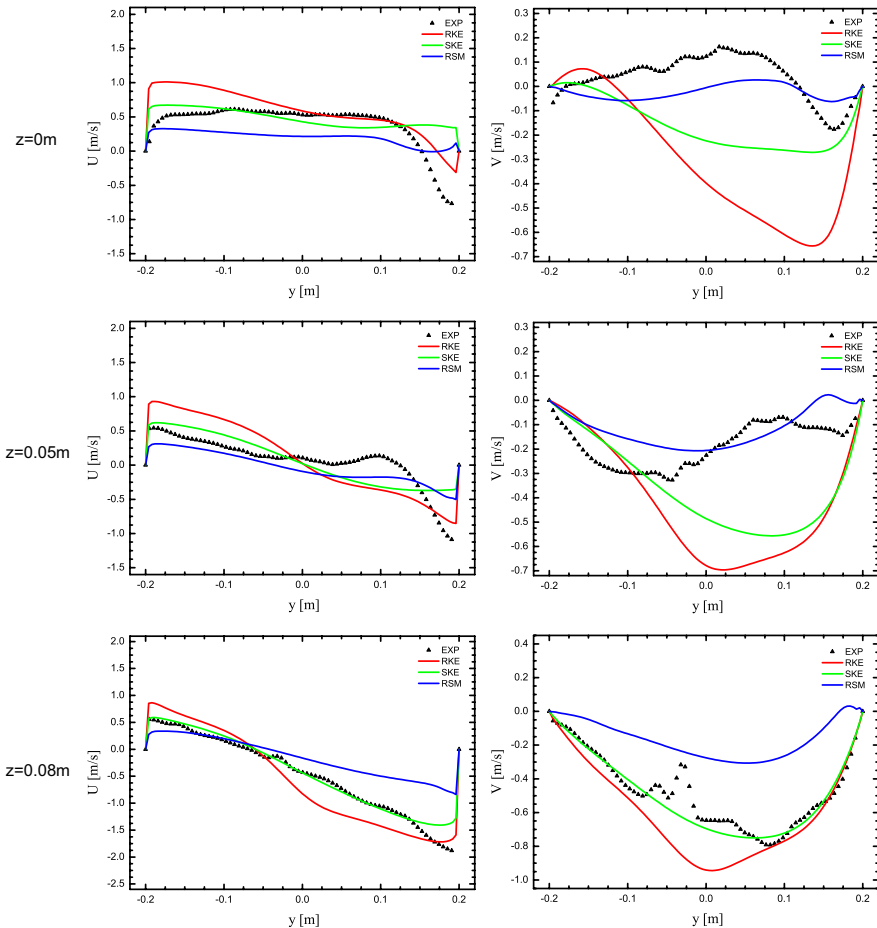
Fig. 10. Comparison for streamwise (left) and wall-normal (right) velocity components along a horizontal line at $z = 0.00$, $z = 0.05$, $z = 0.02$ and the distance 0.2 m ($x = -0.4$) from the left corner of the crossing

numerical data is significant and for streamwise components the difference is especially large in the zone close to the outside wall of the cavity ($y = 0.2$ m). For the wall-normal components, these differences change from one to another cross-cut. Below, one of the indicators characterizing the intensity of the ventilation was used to compare the tested models.

The decay time of marker particles seeded to the flow

In the cavity (zone C), the results of numerical simulations differ significantly from the results of the measurements. Numerical predictions themselves differ significantly depending on the turbulent model used. The accuracy of numerical simulations reflecting real flow changes in the cross-sections of the cavity. In this study, one of the indicators characterizing the efficiency of ventilation was used to compare the calculations with the measurements.
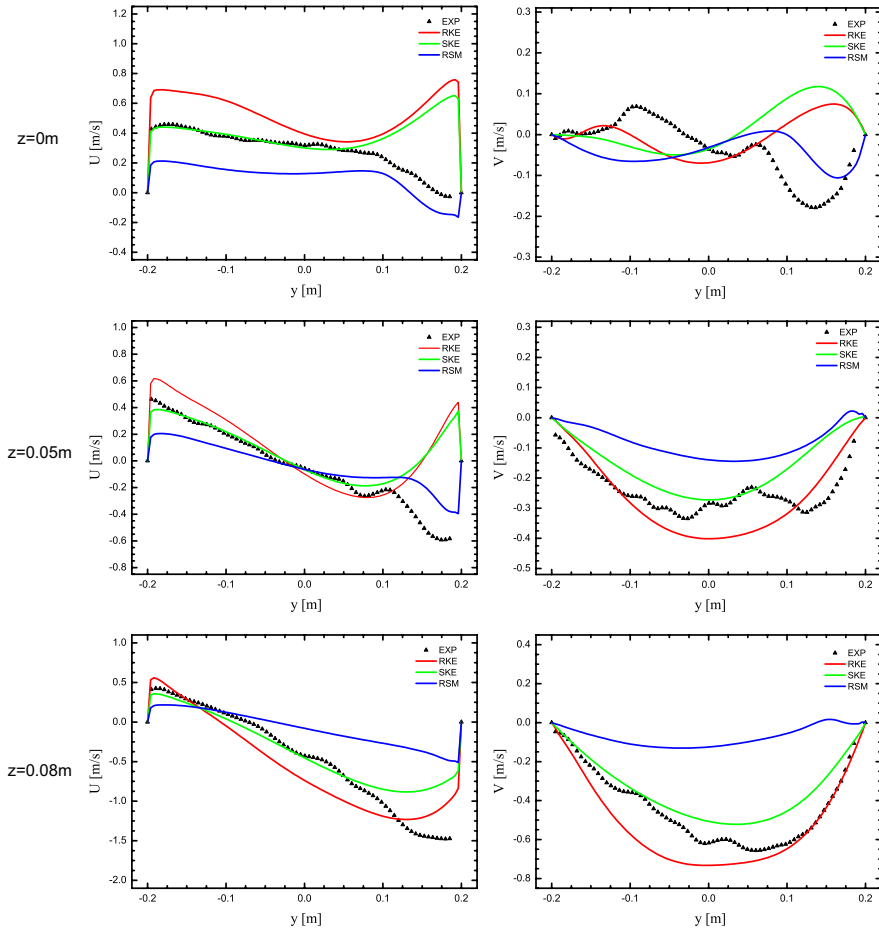
Fig. 11. Comparison for streamwise (left) and wall-normal (right) velocity components along a horizontal line at $z = 0.00$, $z = 0.05$, $z = 0.02$ and the distance 0.3 m ($x = -0.5$) from the left corner of the crossing

An experimental test has been performed for the measurements of the effectiveness of the ventilation phenomena in the cavity. At the back wall of the cavity ($x = -0.7$), a droplets genera-tor (PIV seeding atomiser and oil droplets) was mounted behind the wall and connected to the channel by way of many small holes. This was done to simulate methane injection (distribution) from the wall. After a few injections, the time scale particle concentration in the cavity reaches a statistically steady state.

This allowed us to analyze the performance of the ventilation process in the cavity. It shows the rate at which particle concentration decreases in a chosen cross-section or at any point in the cavity. The concentration of particles is defined as nV_p/V where n is the number of particles in volume V, V_p is a volume of droplets with an average diameter of 1 μm. At the post-processing stage, it was found that the distribution of particles was uniform at the steady state in the cavity. Mean particle concentration at a horizontal plane in the half height of the cavity for the Reynolds
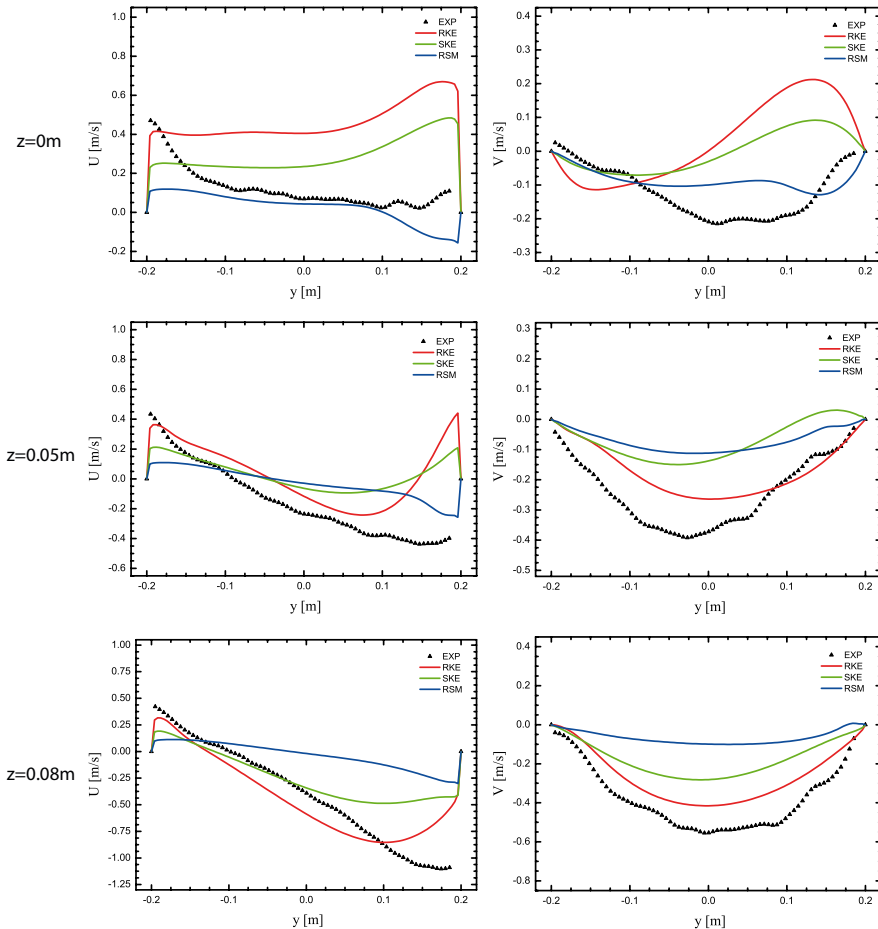
Fig. 12. Comparison for streamwise (left) and wall-normal (right) velocity components along a horizontal line at $z = 0.00$, $z = 0.05$, $z = 0.02$ and the distance 0.4 m ($x = -0.6$) from the left corner of the crossing

number equal to 148,600 is shown in Figure 13. Mean particle concentration is normalized by the particle concentration at the steady-state condition. In the numerical computations, it was assumed that the flow medium creates the ideal mixture of air with the marker particles. The particles have physical properties similar to air. The concentration of markers initially had a constant value throughout the entire area. The software Fluent was also used to calculate variable in time concentration field of markers in the cavity zone. Two turbulent models – standard k-ε and RSM – were used to examine which one predicts the concentration of markers most accurately in comparison with the measured values. Figure 13 shows a comparison of numerical results with experimental data, which is in the range of normalized concentrations from 0.3 to 0.1.

The 'necessary time' for diluting the initial concentration of a marker to a certain level resulting from calculations with the standard k-ε model is 32%-27% shorter than what was determined by the measurements, while RSM model over-predicts the measured results by 18%-27%.
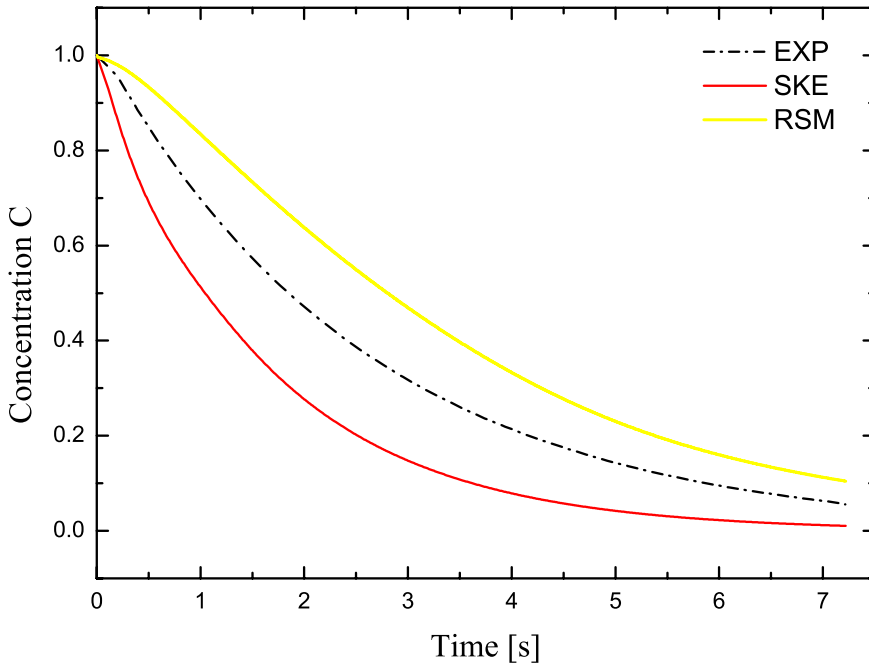
Fig. 13. Mean normalized concentration at a horizontal plane at half depth of the cavity

6. Conclusions

This paper presents the results of the experimental and numerical study of the air flow through a system of T-shape ventilation ducts. None of the developed turbulence models has a universal character; therefore the validation of the particular turbulence model remains a necessary step in the fully justified application.

Three turbulence models, standard *k*-ε, *k*-ε realizable and Reynolds stress model were tested for air flow through a laboratory model of T-shape ducts. The laboratory setup represents a simplified model of the crossing of the longwall and the ventilation gallery. Despite the simple geometry of the flow domain, the structure of the velocity field is complex in this domain. The examined flow is characterized by flow separation, stream impingement on the wall, stress-driven flow and strong streamline curvature.

The research we present allows for the accuracy CFD models to be estimated in order to predict the real transport phenomena in T-shape channel fluid flow. The largest differences between the measured and calculated velocity fields occur in the cavity zone. Neither of the tested models provides fully satisfactory results for the examined flow in the cave zone. Two of the three turbulence models tested—the standard *k*-ε and the *k*-ε realizable—over-predict the measure value of the streamwise velocity components. This will cause the ventilation intensity to be overestimated in this domain. As shown in (Jaszczur et al. 2012a), similar results are obtained with the use of the RNG k-ε model. The RSM model underestimates the measure value of streamwise velocity components and therefore artificially lowers the degree of ventilation in this zone. The indicator

of particle decay time was used to compare the measurements with the calculations. Based on this study, we can conclude that the RSM model provides better predictions than the standard k-ε and k-ε realizable ones do in the cavity zone for the ventilation performance analysis.

The 'necessary time' for diluting the initial concentration of a marker to a certain level resulting from calculations with the standard k-ε model is 32%-27% shorter than what was determined by the measurements, while RSM model over-predicts the measured results by 18%-27%.

Good agreement is achieved between all three turbulence model predictions and measurements in the inflow and outflow sections of the channels, bearing in mind the accuracy needed in ventilation problems.

Acknowledgements

References

Aminossadati S.M., Hooman K., 2008. *Numerical simulation of ventilation air flow in underground mine workings*. 12th U.S./North American Mine Ventilation Symposium, pp. 253-259.

Branny M., Filipek W., 2008. *Numerical simulation of ventilation of blind drifts with a force-exhaust overlap system in condition of methane and dust hazards*. Arch. Min. Sci., Vol. 53, No 2, pp. 221-234.

Haven B.A., Kurosaka M., 1997. *Kidney and anti-kidney vortices in crossflow jets*. Journal of Fluid Mechanics, Vol. 352, pp. 27-64.

Humphery J.A.C., Whitelaw J.H., Yee G., 1981. *Turbulent flow in a square duct with strong curvature*. J. Fluid Mechanics, Vol. 103, pp. 443-463.

Jaszczur M., Portela L., 2008. *Numerical data for reliability of LES for non-isothermal multiphase turbulent channel flow*. Quality and reliability of LES, pp. 343-354.

Jaszczur M, Nowak R., Szmyd J., Banny M., Karch M., Wodziak W., 2011. *An application of SPIV technique to experimental validation of the turbulence model for the air flow in the intersection of the mining face with the ventilation gallery*. Journal of Physics: Conference Series, 318 (5), art. no. 052043.

Jaszczur M., Nowak R., Szmyd J., Banny M., Karch M., Wodziak W., 2012a. *Eksperymentalne i numeryczne badania przepływu powietrza przez skrzyżowanie wyrobisk w kształcie litery T. Zwalczanie zagrożeń aerologicznych w kopalniach*. Katowice, Główny Instytut Górnictwa, pp. 76-87.

Jaszczur M., Nowak R., Szmyd J., Banny M., Karch M., Wodziak W., 2012b. *Experimental validation of the transport phenomena in T-shape channel flow*. Journal of Physics: Conference Series, 395 (1), art. no. 012037.

Kelso R.M., Lim T.T., Perry A.E., 1996. *An experimental study of round jets in cross-flow*. Journal of Fluid Mechanics, Vol. 306, pp. 111-144.

Krawczyk J., 2007. *Jedno i wielowymiarowe modele niestacjonarnych przepływów powietrza i gazów w wyrobiskach kopalnianych. Przykłady zastosowań*. Arch. Min. Sci., Seria: Monografia, nr 2.

Kuan B., Yang W., Schwarz M.P., 2007. *Dilute gas-solid two-phase flows in a curved 90° duct bend: CFD simulation with experimental validation*. Chemical Engineering Science, Vol. 62, pp. 2068-2088.

Mossad R., Yang W., Schwarrz M.P., 2009. *Numerical prediction of air flow in a sharp 90° elbow*. Seventh International Conference on CFD in the Minerals and Process Industries, CSIRO, Melbourne, Australia, pp. 1-5.

Nakayama H., Hirota M., Shinoda K., Koide S., 2005. *Flow Characteristics in a Counter-Flow Type T-junction*. Thermal Science and Engineering, Vol. 13, pp. 17-23.

Rodi W., 1979. *Turbulence models and their application in hydraulics* p. 27 (Delft: IAHR).

Silvester S.A., 2002. *The integration of CFD and VR methods to assist auxiliary ventilation practice*. PhD thesis, The University of Nottingham.

Taylor A.M.K.P., Whitelaw J.H., Yianneskis M., 1982. *Curved ducts with strong secondary motion: velocity measurements of developing laminar and turbulent flow*. Journal of Fluids Engineering, Transactions of the ASME, Vol. 104, Iss. 3, p. 350-359.

Wala A.W., Stoltz J.R., Jacob J.D., 2001. *Numerical and experimental study of a mine face ventilation system for CFD code validation*. Proceedings of the 7th International Mine Ventilation Congress, Krakow, pp. 411-418.

Wala A.M., Vytla S., Taylor C.D., Huang G., 2007. *Mine face ventilation: a comparison of CFD results against benchmark experiments for CFD code validation*. Mining Engineering, Vol. 59, pp. 10-17.